Catal Lett (2008) 123:327–333
DOI 10.1007/s10562-008-9427-3

Catalytic Efficiency of Ceria–Zirconia and Ceria–Hafnia Nanocomposite Oxides for Soot Oxidation

Benjaram M. Reddy · Pankaj Bharali · Gode Thrimurthulu · Pranjal Saikia · Lakshmi Katta · Sang-Eon Park

Received: 3 January 2008 / Accepted: 31 January 2008 / Published online: 14 March 2008

Abstract The catalytic oxidation of soot particulates has been investigated over CeO_2, CeO_2–ZrO_2 and CeO_2–HfO_2 nanocomposite oxides. These oxides were synthesized by a modified precipitation method employing dilute aqueous ammonia solution. The prepared catalysts were characterized by X-ray diffraction (XRD), transmission electron microscopy (TEM), Raman spectroscopy, UV-Vis diffuse reflectance spectroscopy (UV-Vis DRS) and BET surface area methods. The soot oxidation has been evaluated by a thermogravimetric method under 'tight contact' conditions. The XRD results revealed formation of cubic CeO_2, $Ce_{0.75}Zr_{0.25}O_2$ and $Ce_{0.8}Hf_{0.2}O_2$ phases in case of CeO_2, CeO_2–ZrO_2 and CeO_2–HfO_2 samples, respectively. TEM studies confirm the nanosized nature of the catalysts. Raman measurements suggest the presence of oxygen vacancies, lattice defects and oxide ion displacement from normal ceria lattice positions. UV-Vis DRS studies show presence of charge transfer transitions $Ce^{3+}\leftarrow O^{2-}$ and $Ce^{4+}\leftarrow O^{2-}$ respectively. The catalytic activity studies suggest that the oxidation of soot could be enhanced by incorporation of Zr^{4+} and Hf^{4+} into the CeO_2 lattice. The CeO_2–HfO_2 combination catalyst exhibited better activity than the CeO_2–ZrO_2. The observed high activity has been related to the nanosized nature of the composite oxides and the oxygen vacancy created in the crystal lattice.

B. M. Reddy · P. Bharali · G. Thrimurthulu · P. Saikia · L. Katta
Inorganic and Physical Chemistry Division, Indian Institute of Chemical Technology, Hyderabad 500 007, India

B. M. Reddy (✉) · S.-E. Park
Laboratory of Nano-Green Catalysis, Department of Chemistry, Inha University, Incheon 402-751, Republic of Korea
e-mail: mreddyb@yahoo.com

Keywords CeO_2 · CeO_2–ZrO_2 · CeO_2–HfO_2 · Catalyst characterization · Soot oxidation

1 Introduction

Ceria-based (CeO_2) catalysts have been extensively investigated because of their major role in three-way catalysis (TWC) for automotive exhaust-gas purification, fuel cell technology for H_2 production and purification, production of chemicals by selective oxidation and destruction of undesired products by total oxidation, and so on [1–4]. Nevertheless, bulk ceria is not a good catalyst as it exhibits several disadvantages. When exposed to high temperatures the specific surface area of CeO_2 decreases drastically which in turn shrinks its crucial redox properties and oxygen storage/release capacity. Modification of ceria with an appropriate transition or rate earth metal cation improves its stability towards sintering and also oxidation activity of the resulting catalysts [3, 5]. This modification has often been attributed to changes in the redox properties and the creation of oxygen vacancies [5, 6]. Incorporation of Zr^{4+} into CeO_2 lattice has been reported to improve the physicochemical characteristics of ceria and this combination has been applied for various reactions such as preferential oxidation of CO [7, 8], steam reforming of ethanol [9], synthesis of dimethyl carbonate from methanol and CO_2 [10], direct conversion of methane to synthesis gas [11], iso-synthesis [12], dehydration of alcohols [13–17], oxidative dehydrogenation of ethylbenzene [18] and low-temperature water-gas shift reaction [1], apart from the conventional TWC applications to reduce the emissions of noxious pollutants such as CO, NO_x and hydrocarbons from automobile exhausts [2, 19].

Recently ceria-based composite oxides have attracted a lot of attention for oxidation of diesel soot particulates and

reduction of toxic greenhouse gases [6, 20–22]. In particular, the incomplete combustion that occurs in the diesel engines leads to huge emissions of atmospheric pollutants as soot particulates and toxic gases. Soot emission is a significant component of air pollution and is harmful for both human beings and the environment [23]. Among several techniques that have been developed for reducing the emissions from diesel engines, filtering followed by catalytic oxidation is one of the most promising options. This approach is based on the application of a catalyst to achieve the onset of regeneration at a significantly lower temperature [22]. Pertaining to the mechanism involved in the oxidation of soot, several authors have pointed out the significance of redox properties of the catalysts, and the use of cerium oxide materials which confer interesting properties to soot combustion catalysts [22–25]. Catalysts typically employed for soot oxidation should decrease the oxidation temperature (light-off temperature, $T_{1/2}$) and maintain a high activity for longer working periods. The $T_{1/2}$ strongly depends on the contact between the soot and the catalyst [24] and on the specific surface area of the catalytic material [21, 25]. The growth of oxide particles (sintering) during soot oxidation is therefore detrimental to the catalytic activity. It has been reported that gas phase O_2 replenishes the lattice oxygen of ceria creating highly active oxygen, which reacts with soot [26, 27]. Incorporation of La^{3+} significantly improved the catalytic activity of CeO_2 for soot oxidation and this improvement was correlated to an increase in the BET surface area and enhanced redox properties. It has also been reported recently that CeO_2 doped with transition metals (Zr and Fe) and rare earth elements (La, Pr, Sm and Tb) exhibits a high activity for soot oxidation by O_2 [20, 25]. Our recent investigation also revealed that Hf^{4+} incorporated CeO_2 exhibits even better CO oxidation activity than the Zr^{4+} incorporated ceria catalysts [8]. The present investigation has been undertaken against the aforesaid background. In this study structural properties and soot oxidation activity of pure CeO_2, CeO_2–ZrO_2 and CeO_2–HfO_2 composite oxides have been investigated systematically. The synthesized nanocomposite oxides were characterized by X-ray diffraction (XRD), transmission electron microscopy (TEM), Raman spectroscopy (RS), UV-Vis diffuse reflectance spectroscopy (UV-Vis DRS) and BET surface area methods and the soot oxidation measurements were performed by employing a thermogravimetry method.

2 Experimental

2.1 Catalyst Preparation

The CeO_2–ZrO_2 (CZ; 1:1 mole ratio) and CeO_2–HfO_2 (CH; 8:2 mole ratio) composite oxides were synthesized by a coprecipitation method using $(NH_4)_2Ce(NO_3)_6$ (Loba Chemie, GR grade), $Zr(NO_3)_4.5H_2O$ (Fluka, AR grade) and $HfCl_4$ (Aldrich, AR grade) as the precursors and aqueous NH_3 as the precipitating reagent. Pure CeO_2 (C) was also synthesized following the same precipitation method from $(NH_4)_2Ce(NO_3)_6$ (Loba Chemie, GR grade) with aqueous NH_3 solution. The final pH of the solutions was adjusted to $\sim$8.5 for complete precipitation. The obtained precipitates were filtered off and washed several times with doubly distilled water until free from anion impurities, oven dried at 393 K for 12 h and finally calcined at 773 K for 5 h under flowing air atmosphere.

2.2 Catalyst Characterization

The XRD patterns were recorded on a Siemens D−5005 diffractometer using nickel-filtered Cu K_α (0.15418 nm) radiation source. Crystalline phases were identified by comparison with the reference data from PDF-ICDD files. The average crystallite size was estimated using Scherrer equation. The cell '*a*' parameter values were calculated by a standard cubic indexation method using the intensity of the ceria base peak (111). The BET surface areas were obtained by N_2 physisorption at liquid N_2 temperature on a Micromeritics Gemini 2360 instrument. Before measurements, samples were oven dried at 393 K for 12 h and flushed with Argon gas for 2 h. Raman spectra were recorded on a LabRam HR spectrometer equipped with a liquid N_2 cooled CCD detector at ambient temperature and pressure. The emission line at 514.5 nm from an Ar^+ to Kr^+ ion RM 2018 laser was focused on the sample (analyzing spot 1 μm) under the microscope. The power of the incident beam on the sample was 3 mW and time of acquisition varied according to the intensity of the Raman scattering. The UV-Vis DRS measurements were performed over the wavelength range 200–800 nm using a GBS-Cintra 10e UV-Vis NIR spectrophotometer with an integration sphere diffuse reflectance attachment. Samples were diluted in a KBr matrix by pelletization. The TEM images were taken using a JEM-3011 instrument (JEOL) equipped with a slow-scan CCD camera operating at 300 kV. Samples were sonically dispersed in ethanol and deposited on a holey carbon copper grid before examination.

2.3 Activity Measurements

The soot oxidation activity of various catalysts with O_2 was carried out by a thermogravimetric analysis (TGA) method in a Mettler Toledo, TGA/SDTA 851^e instrument. The activity measurements were performed in 'tight contact' (ground in agate mortar) condition with catalyst-soot

mixtures in 4:1 wt/wt ratio [23, 28]. The model soot, Printex U, used in this work was provided by Degussa. A weighed amount of the sample was placed in a TGA crucible and heated to 1,273 K in 100 mL min^{-1} air and the heating rate was 10 K min^{-1}.

3 Results and Discussion

The N_2 BET surface areas of the synthesized C, CZ and CH samples are presented in Table 1. All the samples obtained in the present study by aqueous precipitation method and calcined at 773 K exhibited reasonably high specific surface areas. An increase in the surface areas is noted after incorporation of Zr^{4+} and Hf^{4+} cations into the ceria lattice. The efficacy of Zr^{4+} and Hf^{4+} cations in enhancing the specific surface area of ceria could be related to the variations in the rate of precipitation and crystal growth of the solid solutions formed [29].

The XRD patterns of C, CZ and CH samples are shown in Fig. 1. The diffraction peaks of all the three samples could be indexed to (111), (200), (220), (311), (400), (331) and (420) crystal faces, corresponding to a face centered cubic fluorite structure of CeO_2. As presented in Fig. 1, the formation of a single phase crystalline CeO_2 (PDF-ICDD 34-0394), $Ce_{0.75}Zr_{0.25}O_2$ (PDF-ICDD 28-0271) and $Ce_{0.8}Hf_{0.2}O_2$ (PDF-ICDD 04-006-1933) compounds have been confirmed for C, CZ and CH samples, respectively. It could be further inferred that the slight shift in the peak positions to higher 2θ values in the case of CZ and CH samples indicates the formation of composite oxide phases. Within the detection limits of XRD technique, there is no evidence about the presence of different crystallographic phases of ZrO_2 or HfO_2 [30, 31]. The unit cell parameters have been calculated using the most intense (111) line of CeO_2, $Ce_{0.75}Zr_{0.25}O_2$ and $Ce_{0.8}Hf_{0.2}O_2$ patterns [32, 33]. The evaluation of 'a' cell parameter values of the samples is presented in Table 1. As can be seen from the table, there is a decrease in the lattice parameters in the case of CZ and CH samples. This observation can be attributed to a shrinkage of the ceria lattice due to the replacement of Ce^{4+} (0.97 Å) ions with smaller cations, Zr^{4+} (0.84 Å) or Hf^{4+} (0.78 Å), in agreement with Vegard's law [34, 35]. The decrease in the lattice parameter values can also be taken as an evidence for the formation of composite oxides. The lattice parameter values obtained in the present investigation are in good agreement with earlier reports [36, 37].

Table 1 BET surface area, average crystallite size and lattice parameter measurements of cubic CeO_2, CeO_2–ZrO_2 and CeO_2–HfO_2 samples

Samples	Surface area (m^2g^{-1})	Crystallite size (nm)	Cell parameter '*a*' values (Å)
CeO_2	41	7.3	5.41
CeO_2–ZrO_2	84	4.7	5.35
CeO_2–HfO_2	78	4.6	5.34

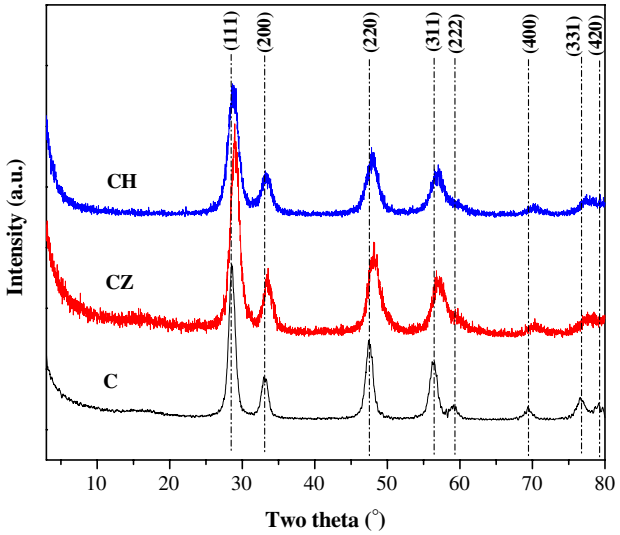

Fig. 1 X-ray diffraction profiles of CeO_2 (C), CeO_2–ZrO_2 (CZ) and CeO_2–HfO_2 (CH) samples

The average crystallite sizes of CeO_2, $Ce_{0.75}Zr_{0.25}O_2$ and $Ce_{0.8}Hf_{0.2}O_2$, obtained by employing Scherrer equation, are found to be in the range of 4–8 nm size (Table 1). As can be noted from Table 1, the incorporation of Zr^{4+} or Hf^{4+} into CeO_2 lattice facilitates an increase in the specific surface areas and the formation of smaller particle sizes. The formation of composite oxides between Ce and Zr or Hf retards the crystallite growth thus paving the way for the formation of thermodynamically more stable phases [38]. TEM studies were performed to confirm the particle sizes obtained from XRD data. The representative TEM images of CZ and CH samples are presented in Fig. 2. It could be noted from the figure that the CZ and CH samples crystallize as cubic fluorite type structure of ceria with particle sizes in the range 4–6 nm. Thus, TEM studies support the observations made from XRD measurements.

Raman spectroscopy has been used for the investigation of catalyst structures, which is a good technique sensitive to both M–O bond arrangement and the lattice defects [3]. Factor group analyses for the ceria fluorite structure (space group *Fm3m*) have been previously performed which indicates that for the cubic structure only one triply degenerate IR active mode is expected, which splits into a transverse optical mode and a longitudinal optical (LO) mode [39, 40]. Also a single Raman active mode (F_{2g}) is anticipated. The spectra of C, CZ and CH samples are presented in Fig. 3 which reveals the absence of bands that correspond to ZrO_2 or HfO_2. This observation suggests that

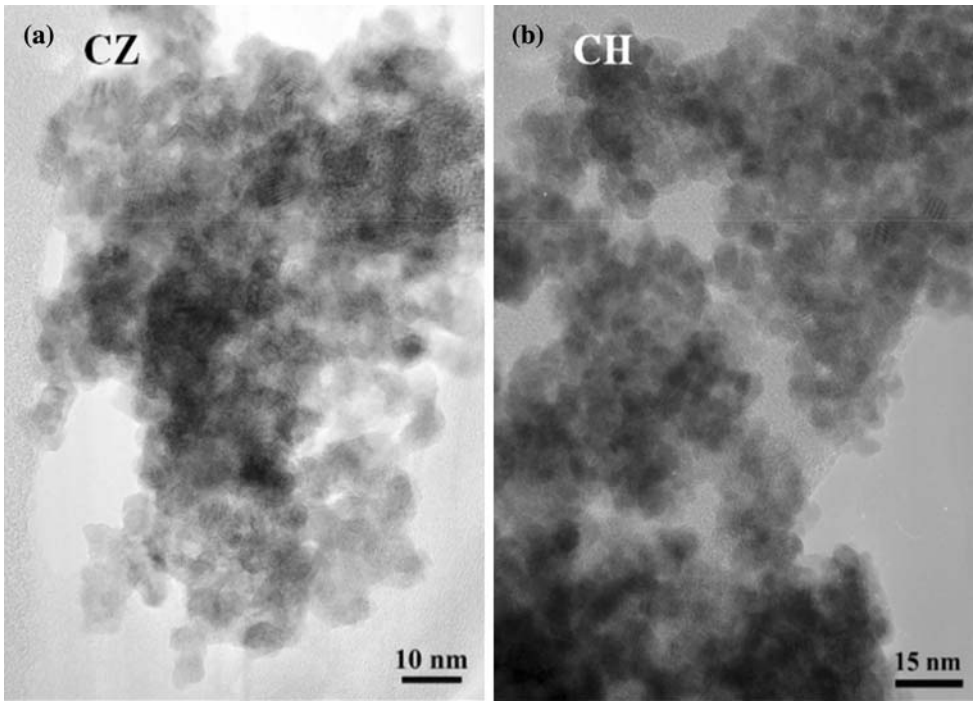

Fig. 2 Transmission electron microscopy images of **a** CeO_2–ZrO_2 (CZ) and **b** CeO_2–HfO_2 (CH) samples

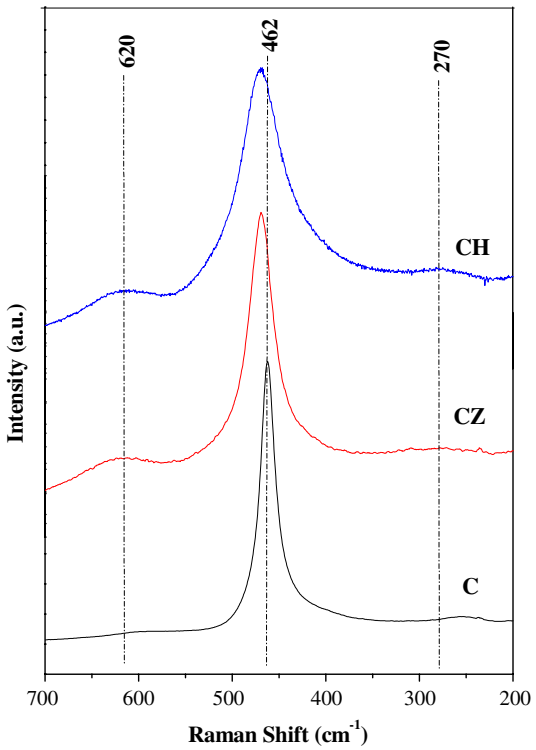

Fig. 3 Raman spectra of CeO_2 (C), CeO_2–ZrO_2 (CZ) and CeO_2–HfO_2 (CH) samples

the Zr^{4+} and Hf^{4+} cations are incorporated into the CeO_2 lattice. The main band of ceria and Zr^{4+} or Hf^{4+} incorporated CeO_2 catalysts at $\sim$462 cm^{-1} is the only allowed Raman mode (F_{2g}) of fluorite-type structure [41, 42]. The F_{2g} band is blue shifted towards higher wave numbers in the case of CZ and CH catalysts. Fluorite-structure is a cubic structure (fcc) in which the cations are placed in the corners and in the centers of faces and oxygen atoms are located at the tetrahedral sites. The Raman spectra for these fluorite-type oxide structures are dominated by oxygen lattice vibrations and are sensitive to the crystal symmetry [42]. In addition to F_{2g} mode, two new broad bands are observed for the CZ and CH samples at $\sim$600 and $\sim$300 cm^{-1}, respectively. The broad band at $\sim$600 cm^{-1} corresponds to non-degenerate LO mode of ceria arising due to relaxation of symmetry rules, which is often linked to oxygen vacancies in the ceria lattice [8, 42, 43]. The other weak band observed at $\sim$300 cm^{-1} could be attributed to the displacement of oxygen atoms from their ideal fluorite lattice positions [40]. The presence of oxygen vacancies or defect sites is expected to enhance the catalytic performance of these systems [8, 30, 44].

The UV-Vis DRS technique has been used extensively to study various metal oxides to obtain information on the surface coordination and different oxidation states of the metal ions by measuring d-d, f-d transitions and oxygen–metal ion charge transfer bands. However, this technique has limitations due to the difficulty in interpreting large bandwidths and specular reflectance often observed in the spectra [36]. According to Bensalem et al. [45], the wavelength corresponding to the UV absorption edge of a semiconducting powder such as CeO_2 can be safely used to probe the presence of nano-crystallites (<5 nm), which cannot be detected by XRD [46]. The DR spectra of C, CZ

and CH samples are shown in Fig. 4. As can be noted from this figure, spectrum of pure CeO_2 exhibits three absorption maxima centered at ~255, 285 and 340 nm. The latter two well-resolved absorption maxima may be caused by $Ce^{4+} \leftarrow O^{2-}$ charge transfer (285 nm) and inter-band (340 nm) transitions [47], whereas the poorly resolved former maxima correspond to $Ce^{3+} \leftarrow O^{2-}$ charge transfer transitions [45]. The absorption edges are slightly red-shifted towards higher wavelengths in the case of CZ and CH samples. Substitution of Zr^{4+} or Hf^{4+} into the CeO_2 lattice and consequent strain development at the cerium sites, due to lowering of symmetry, causes the observed shift towards higher wavelengths [31]. The absorption bands, which correspond to different charge transfer transitions, are poorly resolved in the case of CZ, while the absorption edges are relatively sharp in the case of CH sample. Moreover, the band at ~255 nm, which has been characterized as $Ce^{3+} \leftarrow O^{2-}$ charge transfer transition, is well-resolved in CH compared to C and CZ samples with slight blue-shifted towards lower wavelength. The occurrence of oxygen vacancy defects as noticed from RS studies supports the $Ce^{3+} \leftarrow O^{2-}$ transitions, which is more prominent in the case of CH sample.

The conversion of soot as a function of temperature over the three catalyst samples investigated has been presented in Fig. 5. As can be noted from this figure, all catalysts showed a decreased soot oxidation temperature, as expected. These activity studies have been carried out using air as the source of oxygen in tight contact conditions. We have also performed a few experiments under loose contact conditions. Loose contact did not show a significant decrease in the soot oxidation temperature irrespective of the catalyst employed, which was in agreement with earlier reports [20–22]. Apparently, when the soot particle is not

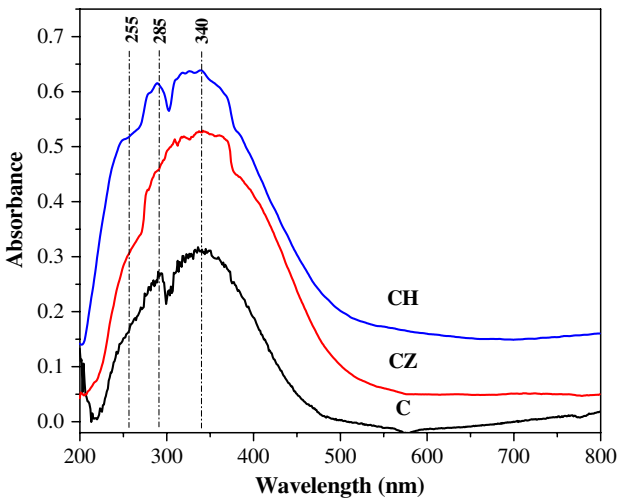

Fig. 4 UV-Vis DRS patterns of CeO_2 (C), CeO_2–ZrO_2 (CZ) and CeO_2–HfO_2 (CH) samples

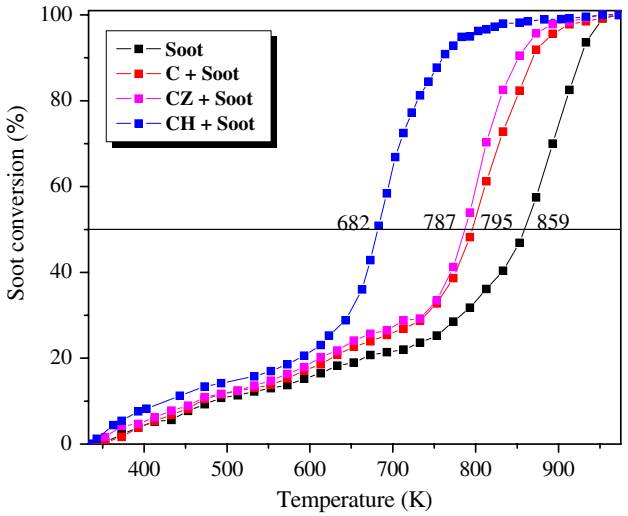

Fig. 5 Conversion of soot versus temperature over CeO_2 (C), CeO_2–ZrO_2 (CZ) and CeO_2–HfO_2 (CH) samples

in close contact with the catalyst surface, the active oxygen cannot be transferred to the soot particle [25, 27, 28]. The active oxygen involved for soot combustion comes from two ways: the gaseous oxygen and the oxygen released from the bulk of the catalysts. The dissociation centers for the adsorption of oxygen provided by the metal oxides also contribute for the observed better catalytic activity [21, 28]. The high catalytic activity of CeO_2 for soot oxidation in air was attributed to the generation of highly active oxygen from the lattice due to the oxygen exchange between gas phase O_2 and oxygen in the oxide framework, as mentioned [21], and the redox cycle Ce^{3+}/Ce^{4+} seems to play an important role in the oxygen exchange process. The light-off temperature (temperature at 50% conversion or $T_{1/2}$) has decreased to a lower value after incorporation of Zr^{4+} and Hf^{4+} cations into the CeO_2 structure. The 50% conversion for bare soot took place at ca. 860 K. But the light-off temperature for the CeO_2−soot mixture has been decreased to 795 K, which further lowered upon Zr^{4+} and Hf^{4+} incorporation. The $T_{1/2}$ temperatures for CZ- and CH-soot mixtures are 787 and 682 K, respectively. This is a significant observation from the present study. It is always desirable to develop better catalysts which could lower the $T_{1/2}$ temperature further. The plausible reasons for an increase in the activity of doped CeO_2 catalysts for soot oxidation have been probed by different characterization techniques in the literature. Among various parameters that were envisaged to explain the differences in catalyzed soot oxidation temperature were catalyst specific surface area, crystallite size, formation of oxygen vacancies in the catalyst structure and low temperature reducibility. In particular, the presence of oxygen vacancies in the CZ and CH samples were identified from Raman and UV-Vis DRS

studies. These results correlate with the activity measurements and are in line with earlier reports [21, 25, 28].

There seems to be a similarity in the behaviour of ceria-based catalysts for oxidation of CO and the soot. A hypothetic mechanism has been envisaged in the literature to explain the same [1, 8, 25, 28]. It is based on the redox mechanism, which utilizes oxygen activated from the support in a typical reduction/oxidation mechanism (Mars–Van Krevelen type) in which the catalyst undergoes a partial reduction. Oxygen storage and release is therefore an important issue because it provides an alternative route for the oxidation of big soot particles. An alternative redox route involves oxygen from the support and gas-phase which reacts with soot to form adsorbed CO_2 in the form of carbonates. Decomposition of carbonate is then stimulated by gas phase oxygen that provides also reoxidation of the support. Irrespective of the mechanism involved, the incorporation of isovalent Zr^{4+} or Hf^{4+} cations into the ceria lattice has been observed to enhance the catalytic activity of ceria for soot oxidation.

4 Conclusions

Nanosized CeO_2, CeO_2–ZrO_2 and CeO_2–HfO_2 composite oxides have been synthesized and characterized by XRD, TEM, Raman, UV-Vis DRS and BET surface area methods. XRD results revealed the formation of cubic CeO_2, $Ce_{0.75}Zr_{0.25}O_2$ and $Ce_{0.8}Hf_{0.2}O_2$ phases in case of CeO_2, CeO_2–ZrO_2 and CeO_2–HfO_2 samples, respectively. The TEM studies confirmed the formation of nanosized CeO_2–ZrO_2 and CeO_2–HfO_2 solid solutions. Raman measurements disclosed the presence of oxygen vacancies, lattice defects and oxide ion displacement from their normal lattice positions. UV-Vis DRS measurements further showed the charge transfer transitions $Ce^{3+}\leftarrow O^{2-}$ and $Ce^{4+}\leftarrow O^{2-}$, respectively. The light-off temperature of the oxidation of model diesel soot particulates significantly decreased after Zr^{4+} or Hf^{4+} ion incorporation into the CeO_2 lattice. The activity results could be related to the defective fluorite structure of the ceria with concomitant formation of oxygen vacancies.

Acknowledgments Thanks are due to Dr S. Loridant, IRCELYON, France for Raman results. B.M. Reddy thanks Korea Federation of Science and Technology (KOFST) for a visiting fellowship under Brain Pool Program. P. Bharali, G. Thrimurthulu, P. Saikia and L. Katta thank Council of Scientific and Industrial Research (CSIR), New Delhi for the research fellowships.

References

1. Trovarelli A (2002) In: Hutchings GJ (ed) Catalysis by ceria and related materials, catalytic science series, vol 2. Imperial College Press, London
2. Trovarelli A, de Leitenburg C, Dolcetti G (1997) Chemtech 27:32–37
3. Monte RD, Kaspar J (2005) J Mater Chem 15:633–648
4. Mackrodt WC, Fowles M, Morris MA (1991) Eur Pat 91:307, 165
5. Matsumoto SI (2004) Catal Today 90:183–190
6. Krishna K, Bueno-Lopez A, Makkee M, Moulijn JA (2007) Appl Catal B Environ 75:189–200
7. Martinez-Arias A, Fernandez-Garcia M, Iglesias-Juez A, Hungria AB, Anderson JA, Conesa JC, Soria J (2001) Appl Catal B Environ 31:51–56
8. Reddy BM, Bharali P, Saikia P, Khan A, Loridant S, Muhler M, Grünert W (2007) J Phys Chem C 111:1878–1881
9. Srinivas D, Satyanarayana CVV, Potdar HS, Ratnasamy P (2003) Appl Catal A Gen 246:323–334
10. Tomishige K, Kunimori K (2002) Appl Catal A Gen 237:103–109
11. Otsuka K, Wang Y, Nakamura M (1999) Appl Catal A Gen 183:317–324
12. Li Y, He D, Zhu Q, Zhang X, Xu B (2004) J Catal 221:584–593
13. Cutrufello MG, Ferino I, Solinas V, Primavera A, Trovarelli A, Auroux A, Picciau C (1999) Phys Chem Chem Phys 1:3369–3375
14. Cutrufello MG, Ferino I, Monaci R, Rombi E, Solinas V (2002) Top Catal 19:225–240
15. Solinas V, Rombi E, Ferino I, Cutrufello MG, Colon G, Navio JA (2003) J Mol Catal A Chem 204–205:629–635
16. Reddy BM, Lakshmanan P, Bharali P, Saikia P (2006) J Mol Catal A Chem 258:355–360
17. Reddy BM, Thrimurthulu G, Saikia P, Bharali P (2007) J Mol Catal A Chem 275:167–173
18. Reddy BM, Lakshmanan P, Loridant S, Yamada Y, Kobayashi T, Lopez-Cartes C, Rojas TC, Fernandez A (2006) J Phys Chem B 110:9140–9147
19. Ozawa M, Matuda K, Suzuki S (2000) J Alloys Compd 303–304:56–59
20. Małecka MA, Kepinski L, Mista W (2007) Appl Catal B Environ 74:290–298
21. Bueno-Lopez A, Krishna K, Makkee M, Moulijn JA (2005) J Catal 230:237–248
22. Zhua L, Yu J, Wang X (2007) J Hazard Mater 140:205–210
23. Liu J, Zhao Z, Xu C, Duan A, Wang L, Zhang S (2007) Catal Commun 8:220–224
24. Neeft J, Makkee M, Moulijn J (1996) Chem Eng J 64:295–302
25. Aneggi E, de Leitenburg C, Dolcetti G, Trovarelli A (2006) Catal Today 114:40–47
26. Bueno-Lopez A, Krishna K, Makkee M, Moulijn JA (2005) Catal Lett 99:203–205
27. Atribak I, Bueno-Lopez A, Garcia-Garcia A (2008) Catal Commun 9:250–255
28. Krishna K, Bueno-Lopez A, Makkee M, Moulijn JA (2007) Top Catal 44–45221–228
29. Kenevey K, Valdivieso F, Soustelle M, Pijolat M (2001) Appl Catal B Environ 29:93–101
30. Reddy BM, Lakshmanan P, Bharali P, Saikia P, Thrimurthulu G, Muhler M, Grünert W (2007) J Phys Chem C 111:10478–10483
31. Reddy BM, Khan A (2005) Catal Surv Asia 9:155–171
32. Bozo C, Gaillard F, Guilhaume N (2001) Appl Catal A Gen 220:69–77
33. Colon G, Pijolat M, Valdivieso F, Vidal H, Kaspar J, Finocchio E, Daturi M, Binet C, Lavalley JC, Baker RT, Bernal S (1998) J Chem Soc Faraday Trans 94:3717–3726
34. Yashima M, Arashi H, Kakihana M, Yoshimura M (1992) J Am Ceram Soc 75:1541–1549
35. Shannon RD (1976) Acta Crystallogr A 32:751–767
36. Weckhuysen BM, Schoonheydt RA (1999) Catal Today 49:441–451
37. Gao X, Wachs IE (2000) J Phys Chem B 1041261–1268

38. Reddy BM, Khan A, Yamada Y, Kobayashi T, Loridant S, Volta JC (2003) Langmuir 19:3025–3030
39. Hirata T, Asari E, Kitajima M (1994) J Solid State Chem 110:201–207
40. Escribano VS, Lopez EF, Panizza M, Resini C, Amores JMG, Busca G (2003) Solid State Sci 5:1369–1376
41. Shyu JZ, Weber WH, Gandhi HS (1988) J Phys Chem 92:4964–4970
42. Martinez-Arias A, Fernandez-Garcia M, Salamanca LN, Valenzuela RX, Conesa JC, Soria J (2000) J Phys Chem B 104: 4038–4046
43. Weber WH, Hass KC, McBride JR (1993) Phys Rev B 48:178–185
44. Fujimori H, Yashima M, Sasaki S, Kakihana M, Mori T, Tanaka M, Yoshimura M (2001) Phys Rev B 64:134104-1–134104-5
45. Bensalem A, Bozon-Verduraz F, Delamar M, Bugli G (1995) Appl Catal A Gen 121:81–93
46. Zaki MI, Hussein GAM, Mansour SAA, Ismail HM, Mekhemer GAH (1997) Colloids Surf A Physicochem Eng Asp 127:47–56
47. Bensalem A, Muller JC, Bozon-Verduraz F (1992) J Chem Soc Faraday Trans 88:153–154